Journal of IoT in Social, Mobile, Analytics, and Cloud (ISSN: 2582-1369)
www.irojournals.com/iroismac/

Detection of White Blood Cell Cancer using Deep Learning using Cmyk-Moment Localisation for Information Retrieval

M. Muthumanjula[1], Ramasubramanian Bhoopalan[2]

[1]PG Scholar, SRM TRP Engineering College, Trichy, TamilNadu, India
[2]Professor, Department of ECE, SRM TRP Engineering College, Trichy, TamilNadu, India

E-mail: [1]muthumanjula1997@gmail.com, [2]ramatech87@gmail.com

Abstract

Medical diagnosis, notably concerning tumors, has been transformed by artificial intelligence as well as deep neural network. White blood cell identification, in particular, necessitates effective diagnosis and therapy. White Blood Cell Cancer (WBCC) comes in a variety of forms. Acute Leukemia Lymphocytes (ALL), Acute Myeloma Lymphocytes (AML), Chronic Leukemia Lymphocytes (CLL), and Chronic Myeloma Lymphocytes (CML) are white blood cell cancers for which detection is time-consuming procedure, vulnerable to sentient as well as equipment blunders. Despite just a comprehensive review with a competent examiner, it can be hard to render a precise conclusive determination in some cases. Conversely, Computer-Aided Diagnosis (CAD) may assist in lessening the number of inaccuracies as well as duration spent in diagnosing WBCC.

Though deep learning is widely regarded as the most advanced method for detecting WBCCs, the richness of the retrieved attributes employed in developing the pixel-wise categorization algorithms has a substantial relationship with the efficiency of WBCC identification. The investigation of the various phases of alterations related with WBC concentrations and characteristics is crucial to CAD. Leveraging image handling plus deep learning technologies, a novel fusion characteristic retrieval technique has been created in this research. The suggested approach is divided into two parts: 1) The CMYK-moment localization approach is applied to define the Region of Interest (ROI) and 2) A CNN dependent characteristic blend strategy is utilized to obtain deep learning characteristics. The relevance of the retrieved characteristics is assessed via a variety of categorization techniques. The suggested component collection approach versus different attributes retrieval

DOI: https://doi.org/10.36548/jismac.2022.1.006
Received: 26.03.2022, received in revised form: 17.04.2022, accepted: 03.05.2022, published: 16.05.2022

techniques is tested with an exogenous resource. With all the predictors, the suggested methodology exhibits good effectiveness, adaptability, including consistency, exhibiting aggregate categorization accuracies of 97.57 percent and 96.41 percent, correspondingly, utilizing the main as well as auxiliary samples. This approach has provided a novel option for enhancing CLL identification that may result towards a more accurate identification of malignancies.

Keywords: ALL, AML, CLL, CML, WBCC, deep learning, CNN, ROI

1. Introduction

Information aspects like categorization as well as grouping are defined using characteristics, which are information identifiers. Readily distinguishable among different kinds of leukemia and myeloma requires a thorough knowledge of WBC characteristics. Although computerized but also physical procedures are utilized to identify, segregate, then classify WBCs, contemporary techniques confront significant obstacles [1]. WBC identification is done manually by examiners and is prone to sentient fault, resulting in incorrect findings. It is indeed a difficult, moment taken process that is vulnerable to interethnic as well as intra-class heterogeneity between examiners. Just 76.6 percent of instances had pathologists concur on the assessment [2]. In 2019, over 1500 individuals dead as a result of this condition, accounting for 0.2 percent of all cancer-related mortality [3]. Further issues stem from WBCs' complicated composition, such as uneven margins and tactile resemblance among WBCs and additional blood constituents that make it challenging to distinguish WBCs in various blood elements. [4].

WBCs come in a variety of subgroups, comprising both healthy and malignant units [5]. Furthermore, differences in marking as well as exposure make WBC recognition extremely complex [6].Nevertheless, most laboratory-based robotic WBC identification approaches concentrate on statistical instead of subjective picture analysis as well as feature identification techniques [7]. Conventional machine learning (CML) as well as deep learning (DL) approaches been extensively employed for a variety of purposes, including clinical imagery assessment (CIA) [8]. CIA works with a variety of imaging sources, including MRI, CT-Scan, and X-Ray. Ultrasounds, Positron Emission Tomography (PET), blood smear pictures, and fusion paradigms are all examples of imaging techniques [9]. As a result, the creation of robust and adaptable training methods can be facilitated by the introduction of

novel computer-aided techniques for precise WBC identification. A novel characteristic retrieval technique for WBC identification was suggested in this work. A blended CMYK localization approach relying on image analysis as well as a deep learning information integration technique employing a CNN is presented. The suggested approach can also be utilized to create a conceptual delineation framework that will assist examiners in recognizing as well as pinpointing WBCs, which will aid enhance identification efficiency.

2. Related Works

WBC detection is difficult due to the complicated structure of cellular pictures that renders identifying important WBC traits increasingly complex. To distinguish WBCs from different blood constituents, investigators have endeavored to isolate but instead define key properties of WBCs. Customized characteristics as well as deep learning dependent features are the two sorts of WBC attributes. Image analysis technologies are used to create customized characteristics, which are then combined with typical machine-learning (ML) strategies. Deep learning-based characteristics, on the other hand, are automatically derived includes from deep learning systems that can be employed with fully connected tiers (as element of a deep learning framework) nor coupled to an exterior machine learning algorithm. Several scholars have demonstrated outstanding effectiveness using customized characteristics that accomplish WBC identification as well as fragmentation [10] – [16]. Nevertheless, when it comes to handling complicated issues, such approaches have significant limits in regards of accuracy [17]. Furthermore, in perspective of scalability for addressing intricate challenges, those strategies have significant constraints [18].

To construct a WBC differentiation program, Lu et al. [19] utilized a feature encoder employing remnant chunks to retrieve as well as merge multistate characteristics. Researchers further enhanced the WBC delineation overlay by using convolution as well as deconvolution decoders. Neutrophils, eosinophil, basophils, monocytes, and lymphocytes were used to test their approach on four databases of healthy WBCs. In comparison to previous comparison approaches, this method yielded the superior outcomes. Roy et al. [6] suggested a technique for extracting white blood cell (WBC) characteristics utilizing the DeepLabv3+ framework and a ResNet-50 featured harvester. After that, the retrieved characteristics were leveraged to create a WBC partitioning mechanism. The algorithm was tested on three distinct open resources that obtained a segment efficiency of 96.1 percent.

To locate WBCs utilizing the closeness degree of characteristics among WBCs, Abdurrazzaq et al. [20] employed a solitary value decomposition procedure. When contrasted to previous methodologies, their findings revealed an enhancement in WBC cores identification and also WBC recognition, especially for WBCs having moderate color strength. This approach has a separation efficiency of 63 percent on general. For generate ROIs for WBC fragmentation, Khomairoh et al. [21] employed the Haar cascade paradigm for WBC characteristic retrieval. The prototype was created with a sample of M4, M5, and M7 AML subgroups, with characteristics retrieved via various convolution kernels such as edges, lines, plus four-rectangle kernels. Following that, for core and mitochondrial delineation, a color-based technique was applied. Core delineation accuracy rate for M4, M5, and M7 were 87.5 percent, 90.4 percent, and 84.6 percent, correspondingly. The program, on the other hand, attained total accuracy rate of 75 percent, 71.4 percent, and 80.76 percent for mitochondrial delineation for M4, M5, and M7, accordingly. Hegde et al. [22] used a CNN to evaluate the effectiveness of customized features to deep learning characteristics. Geometry, hue, as well as roughness were among the customized characteristics examined, and deep-learning-based characteristics were derived from AlexNet's fc6, fc7, and fc8 tiers. A neural network (NN) algorithm was used to contrast the two techniques. All strategies yielded similar findings, with a 99 percent total efficiency.

Saleem et al. [23] extracted WBC characteristics for sequential fragmentation and categorization using attributes merging with DarkNet-53 and ShuffleNet, as well as obtained 98.6 percent segmented efficiency.Ramya et al. [24] used sliced WBCs to obtain a series of picture intensities and analytical parameters for categorization into AML and healthy. Hue, structure, and a gray-level co-occurrence matrix (GLCM) were among the retrieved characteristics. To tackle the issue of the baseline outline in the level-set splitting methodology, Rad et al. [25] created a novel entity identification strategy using empirical as well as anatomical data. Researchers developed an artificial region-based baseline outline using numerical plus anatomical characteristics both within as well as exterior the outline. The approach had a 96 percent accuracy rate, was tested by two foreign samples, and produced the best findings. To retrieve the regional picture attributes for WBC identification, Puigdollers et al. [14] employed a bag-of-words technique. Their technique had an accuracy rate of 80% and did hardly demand precisely built characteristics to pinpoint WBCs, rendering it easier to use yet relatively broad.

Hue and numerical characteristics were retrieved by Loddo et al. [26] in order to build a multiple categorization algorithm relying on an SVM plus KNN. Hue characteristics were determined pixel by pixel utilizing a 3× 3 pixel community to average the RBG image of every pixel. The approach was refined to build a WBC enumeration method utilizing a round Hough transformation that reached 99.7% reliability [27].

WBC characteristic retrieval has mainly concentrated on healthy WBCs and Chronic Leukemia Lymphocytes (CLL) according to the study. Yet, due to a number of obstacles, only a small amount of study has been done on the identification of WBCs acquired from CLL individuals. As a result, the emphasis of this research is on characteristic retrieval with a variety of WBCs, comprising healthy WBCs and WBCs derived from CLL microscopic pictures. The foregoing are the additions to the research made by this research:

1. We created a novel WBC mapping approach called CMYK-moment localization, which is centered on the CMYK hue field conversion and picture instances.

2. We developed a novel CNN-based component harvest technique relying on characteristic fusion of point wise plus specialized characteristics by merging a deep tier with a profound piled tier to recover generic characteristics while preserving the authenticity of pixel data.

3. For CMYK-moment localization, we suggested a mixed WBC component retrieval paradigm relying on component union as well as CNN-based component retrieval.

3. Methods

3.1 Dataset

A unicellular morphology sample of lymphocytes of individuals with CLL and healthy counterparts was employed in this investigation. The primary dataset contains 377 malignant lymphoma samples with tagged pictures [28]. CLL, Follicular Lymphoma (FL), and Mantle Cell Lymphoma (MCL) are among the three forms of cancers represented in these databases.113 CLL samples were taken from those samples for this study. Figure 1(a) illustrates the many forms of lymphoma.

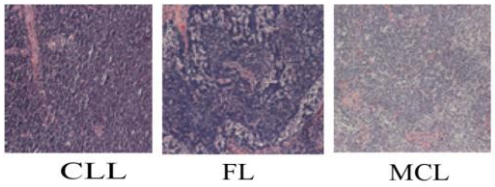

Figure 1(a). Forms of lymphoma

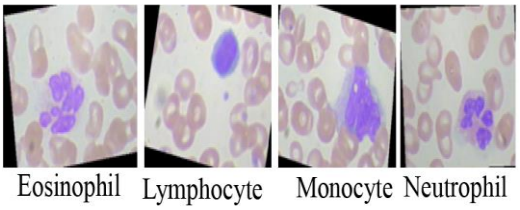

Figure1(b). Components of WBC

Another collection of photos has 9,957 photographs of Eosinophils, Lymphocytes, Monocytes, and Neutrophils. Lymphocytic images were identified in 2,483 of the pictures. These samples are used to assess the model's effectiveness. To assess the model's effectiveness, a supplementary sample of 17,092 healthy radial blood specimens from human cells was employed. The sample was created in RGB hue scheme with CellaVision DM96. An professional physician classified the photos, which were created in RGB hue scheme, jpg style, and 360 × 363 measurements. Segmented neutrophils, eosinophils, basophils, lymphocytes, monocytes, erythroblasts, metamyelocytes, myelocytes, promyelocytes, and platelets are among the eight kinds of red plasma cell in the collection [29].

3.2 Proposed Model

The suggested component retrieval approach combines the CMYK-moment localization with CNN information merging techniques. The CMYK-moment localization technique was employed in this work to retrieve the ROI by combining the hue modification technique (CMYK) with picture occurrences. An ROI was utilized to limit the quantity of unnecessary data in order to recover context free WBC characteristics that are solely dependent on WBC units, that aids in the discovery of more basic WBC characteristics which could be utilized to identify various kinds of WBCs [21].

Overfitting is reduced while calculation duration is reduced by removing superfluous data. Due to the obvious intricate biotic essence of WBCs, like their structure, contour, hue, intensity discrepancies, anomalous borders, as well as compositional resemblances among

WBCs and some blood elements, retrieving characteristics that can effectively recognize various kinds of WBCs as well as distinguish among WBCs as well as some blood elements is daunting.

When opposed to traditional roughness information retrieval approaches, including such Gabor screens, deep CNN convolutional screens can recover complicated texturing features. CNN convolutional screens have indeed been discovered to operate well with photos compared with alternative forms of input in particular [30].There were four tiers in the suggested CNN information blending paradigm. The source tier for RGB pictures is the initial tier, accompanied by dual convolutional tiers. The initial tier is made up of twin tiers: a solitary point wise overlay with a piled spatial overlay. The initial convolutional tier aids in the retrieval of simple characteristics like edges, while the subsequent tier aids in the retrieval of highly complicated structures like texture characteristics. Sequence I (ROI identification), Sequence II (component retrieval), plus sequence III (System testing) were the four sections of the hypothesized characteristic harvesting technique. Figure 2 illustrates the recommended strategy.

3.2.1 Sequence I: ROI IDENTIFICATION

Employing the CMYK instant mapping technique, a ROI was generated in this stage. RGB pictures are transformed to CMYK hue code using this technique. The C path was again removed, and a binary overlay was created using the Otsu thresholding approach to retrieve the WBC core. To eliminate disconnected elements and generate an improved binary overlay, subsequent treatment methods were used, including morphology aperture as well as optimum linked area (OLA).The core' epicenter was then estimated via image analysis. Applying the continuity formula, the core location was estimated:

$$S_{xy} = \sum_a \sum_b a^x b^y k(a,b) \tag{1}$$

$$P_A = \frac{S_{10}}{S_{00}} \tag{2}$$

$$P_B = \frac{S_{01}}{S_{00}} \tag{3}$$

The picture strength is$k(a,b)$, and the x and y axes are $P_A$andP_B, correspondingly. A ring was drawn about the epicenter to calculate the greatest circumference of WBCs. To retrieve the ROI, a squared polygon was formed surrounding the ring, as shown in Figure 3.

3.2.2 Sequence II: ATTRIBUTE RETRIEVAL

The ROI pictures were tagged in this step to indicate WBCs in the frontline as well as similar blood constituents in the backdrop. Then, employing attribute merging of pointwise and localized characteristics, 2D CNN convolutional strands were employed to collect characteristics.

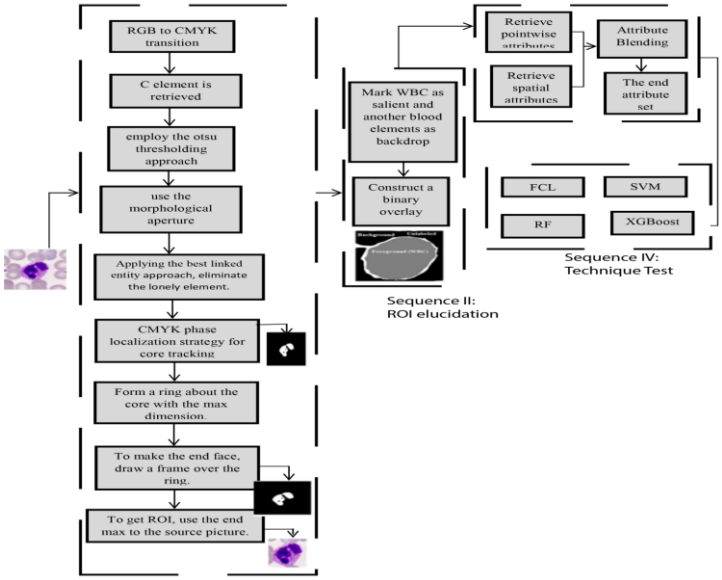

Figure 2. The suggested WBC Attribute retrieval approach paradigm

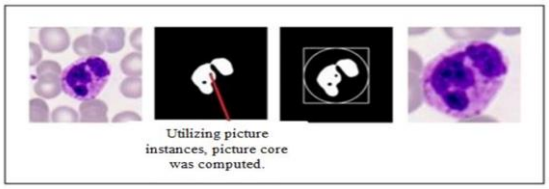

Figure 3. ROI retrieved with CMYK-moment localization approach

Algorithm: Suggested Attribute Retrieval approach.

1. Peruse RGB picture as K(a,b).
2. **Calculate the picture aspects of K(a,b):**
   U = width of K(a,b).
   V= altitude of K(a,b).
3. **Specify the outcome type grades as follows:**
   WBC=1.
   Non-WBC=0.
4. **Transform to CMYK:**
   CALL Convert_To_CMYK with present picture K(a,b).
5. Retrieve C conduit
6. Transform the picture to grayscale.
7. **Pertain Otsu Thresholding:**
   With a histogram, compute the likelihood for every picture strength threshold.
   For x = 0 to U
   For y = 0 to V
   Compute probability strength p(K(a,b))
   Establish the yield class probabilities.

Establish the yield class means.
M = Thresholds' realm
WCV = 0
For t = 1 to M:
For x = 0 to 1:
Compute w_x
Compute σ_x
Compute within-class variance WCV_x as $WCV_x = w_x\sigma_x$
WCV[x] WCV_x
End for
Compute within-class variance WCV as $WCV_t=\sum_{x=0}^{1} WCV[i]$
WCV[t] WCV_t
End for
T_{final}=min(WCV[t])
If K(x,y) <T_{final}:
K(x,y) = 0
Else
K(x,y) = 1.

8. **Use Morphological Aperture:**
S(4,4) ← Architectural component of 4
O ← Aperture action.
Θ ← Erosion action.
$\oplus$ ← Dilation action.
K(x,y) o S(4,4) = K(x,y) Θ (S(4,4) $\oplus$ S(4,4))
9. **Compute the MCR:**
Identify the picture upon morphological aperture, lumps.
Compute the dimension of every lump.
Choose the lump with maximal dimension as WBC core.
10. **Generate a fresh picture with the WBC core that was retrieved.**
11. **Picture impulses are used to compute the core Centro.**

$$S_{xy} = \sum_{a}\sum_{b} a^x\, b^y k(a,b)$$

Compute the x-axes of the picture Centro as $P_A = \frac{S_{10}}{S_{00}}$
Compute the y-axes of the picture Centro as $P_B = \frac{S_{01}}{S_{00}}$

12. **Compute the maximal WBC circumference d.**
13. **A ring (R) should be made over the core with $(\boldsymbol{a} - \boldsymbol{P_A})^2 + (\boldsymbol{b} - \boldsymbol{P_B})^2 = \boldsymbol{d^2}$.**
14. **A square (W) should be made over the R with a side extend of d.**
15. **ROI← W.**
16. **Retrieve 64 pointwise CNN attributes from ROI:**
$h_y(A)$ ← The x[th] attribute maps.
$g_{xy}(A)$← The kernel action of dimension 1×1.
f_x ← ROI Source
$h_y(A) = \sum_{x=1}^{64} f_x \otimes g_{xy}(A)$.
17. **Retrieve 64 exceptional CNN attributes from ROI:**
$k_y(A)$ ← The x[th] attribute maps.
$g_{xy}(A)$← The kernel action of dimension 3×3.
f_x ← ROI Source
$k_y(A) = \sum_{x=1}^{64} f_x \otimes g_{xy}(A)$.
18. **Stack the retrieved pointwise and the exceptional attributes:**
$c_y(A) = h_y(A) + k_y(A)$

Convolutional layers are important components of a CNN framework, and they are made up of an array of kernels that are employed to interpolate the source picture and send it to the upper tiers with the calculation:

$$h_y(A) = \sum_{x=1}^{R} f_x \otimes g_{xy}(A) \quad (4)$$

$h_y(A)$ indicates the j[th] attribute maps created by convolutioning the source picture at the particular position A = (i,j); $g_{xy}(A)$ indicates the kernel among the f_x source channel plus

the h_y attribute map; as well as the ⊗ indicates the convolution action which can be denoted as:

$$f_x \otimes g_{xy}(i,j) = \sum_s \sum_t f_x(s,t) g_{xy}(i-s)(j-t) \quad (5)$$

Convolutional levels are utilized to understand the attributes of the source picture, which range from simple to complicated. The CNN's layer is intended to acquire simple attributes like edge characteristics that are akin to Gabor filter characteristics but the inner tiers are intended to acquire more intricate designs like contour characteristics. Convolution stacks, on the other hand, can be regarded an improved contour element retrieval method when contrasted to the Gabor approach.

Table1. Categorization outcome of the suggested characteristic retrieval approach via primary sample

Primary Sample	Kind of categorizer	No. of attributes	Accuracy	Sensitivity	Specificity	Precision	F-Score	AUC	Jaccard Index	Duration (Secs)
Suggested Procedure	SVM	133	0.98	0.96	0.95	0.98	0.97	0.97	0.95	38.7
	FCL	133	0.97	0.96	0.95	0.99	0.98	0.97	0.95	697.5
	RF	133	0.97	0.97	0.96	0.98	0.98	0.97	0.95	1256.5
	XGBoost	133	0.97	0.96	0.95	0.99	0.97	0.97	0.95	1153.5

Table 2. Categorization outcome of the suggested characteristic retrieval approach via secondary sample

Secondary Sample	Kind of categorizer	No. of attributes	Accuracy	Sensitivity	Specificity	Precision	F-Score	AUC	Jaccard Index
Suggested Procedure	SVM	133	0.96	0.98	0.97	0.95	0.96	0.96	0.93
	FCL	133	0.95	0.94	0.93	0.96	0.95	0.95	0.90
	RF	133	0.95	0.96	0.96	0.95	0.95	0.95	0.91
	XGBoost	133	0.95	0.94	0.94	0.96	0.95	0.95	0.91

The convolution structure's source is a three-channel picture with the dimensions 3×T×E, while the outcome is a characteristic chart with the dimensions F×T'×E', in which F is the quantity of outlet screens and T' and E' are the thickness and elevation of the outlet screens, accordingly. Consider that kt and ke are the thickness and elevation, correspondingly, of the convolution field. The values of T' can be measured with T' = T-kt +1 and the value of E' can be measured with E'=E-ke + 1. The distinct screen loads of the three source streams (R, G, and B) were added to get every screen in the resultant characteristic chart [31],[32].The characteristics were recovered in this work utilizing 2D discrete convolution, with every network's characteristics retrieved individually. After that,

employing point - wise convolution, the collected characteristics were pooled across the three streams. The design was made up of two tiers that ran parallel to each other.

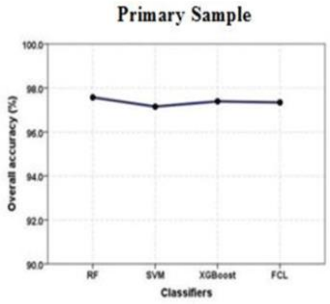

Figure 4. Suggested characteristic retrieval approach's accuracy on primary sample set.

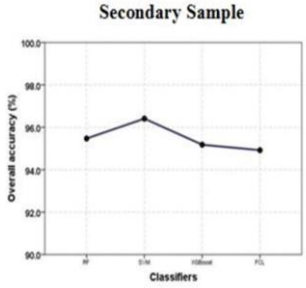

Figure 5. Suggested characteristic retrieval approach's accuracy on secondary sample set.

The initial tier is a 64-filter point - wise convolution stage having a 1×1 kernel dimension and a LeakyReLU activation unit having alpha = 0.3, accompanied by a two ordinary pooling structure. The below solution represents the leakyReLU stack:

$$P_c^v(y) = \max(L_c^v(y), L_c^v(y)x0.3) \quad (6)$$

Since implementing the LeakyReLU activation code, $P_c^v(y)$is the pixel score at position y of the c^{th} stream and v^{th} convolution stage. The continuity formula can be used to describe optimal pooling:

$$A_c^v(y) = \frac{1}{P_h P_w} \sum_{x=1}^{x=P_h P_w} P_c^v\,(x) \quad (7)$$

Where$A_c^v(y)$ is the pixel at position y following the average pooling process; P_h and $P_w$are the picture elevation as well as thickness, accordingly; and $P_c^v(x)$ is the pixel at position x following the LeakyReLU activation operation.

Due to the many convolutional procedures, the point - wise level was employed to retrieve low-level characteristics avoiding the sacrifice of pixel data. The second tier was a piled tier made up of dual convolutional tiers of 64 screen with a 3×3 kernel and a 0.3 alpha coefficient LeakyReLU activation unit. To prevent overfitting, the convolution tiers being preceded by average pool and a 20% ejection tier [33]. To keep the outcome fitters the identical aspect as the source photographs, a zero-padding approach was used on the source pictures. Upon those original images, a zero-padding method was applied to preserve the end fitters the same proportion as the reference shots. The recommended characteristic retrieval theory's methodology is shown. Upon eliminating the untreated information, the retrieved characteristics were plotted to the relevant binary tags to produce the end sample for network development.

3.2.3 Sequence III: Algorithm Critique

Numerous categorization methods were used to test the suggested characteristic retrieval approach on two corpora: primary as well as secondary. Prototype learning and validation were done on the primary sample; meanwhile assessment was done on the secondary set of records. Fully connected layers (FCL) [34], random forest (RF) [35], support vector machine (SVM) [36], and XGBoost [37] were among the categorization techniques used to examine the methods. Overall accuracy, sensitivity, precision, specificity, F-score, area under the receiver operating characteristic (ROC) curve (AUC), and intersecting over unification (IoU) were used to evaluate categorization effectiveness [38]–[40]. The proportion of accurately categorized pixels is measured by the total accuracy. The sensitivity, often referred as the true positive (T_Pos) proportion, is a measurement of the percentage of accurately recognized WBC cells. The true negative (T_Neg) value, which quantifies the properly categorized non-WBC cells, is often referred as specificity. Specificity is typically alluded to as the true negative (TN) score that counts the correctly classified non-WBC units. As a result, the F-score gives an unified metric of precision and sensitivity, and would be especially relevant for situations involving unbalanced information categorization. Various thresholds are used to assess algorithm effectiveness in the AUC. The IoU, also known as the Jaccard index [38], is a popular tool in the domain of entity identification for determining the resemblance among an anticipated entity with its associated underlying reality. The effectiveness metrics were calculated using Formulas (8) – (14) as actually follows:

$$Total\ Accuracy = \frac{T\_Pos+T\_Neg}{T\_Pos+F\_Neg+F\_Pos+T\_Neg} \quad (8)$$

$$Precision = \frac{T\_Pos}{T\_Pos+F\_Pos} \quad (9)$$

$$Sensitivity = \frac{T\_Pos}{T\_Pos+F\_Neg} \quad (10)$$

$$Specificity = \frac{T\_Neg}{T\_Neg+F\_Pos} \quad (11)$$

$$F1 - Score = 2 * \frac{Precision*Sensitivity}{Precision+Sensitivity} \quad (12)$$

$$AUC = \frac{Sensitivity+Precision}{2} \quad (13)$$

$$IoU = \frac{T\_Pos}{F\_Pos+F\_Neg+T\_Pos} \quad (14)$$

The system was build and executed on the Intel Corei7 processor with 2.60 GHz 192 with a 64-bit operating system having 16 GB of RAM with a max-design. To retrieve custom characteristics, the method was constructed in Python and used the Keras deep learning module as well as additional image-processing programme.

4. Results and Discussion

Every pixel was categorized as forefront (WBC) or backdrop (different blood constituents) using a collection of 128 characteristics. The collection had 3,192,550 pixels, with 1,795,988 pixels identified as forefront (56.3 percent) and 1,396,562 pixels labeled as backdrop (43.7 percent). The collection was subsequently split into two parts for learning and evaluating: 80% and 20%, accordingly. The outcomes of the four assessment techniques indicated in Section III are listed below.

4.1 Primary Sample

With FCL, RF, SVM, and XGBoost, the suggested characteristic harvesting approach attained total accuracy of 0.97,0.98, 0.97, and 0.98 correspondingly. The suggested characteristic retrieval strategy produced consistent outcomes for various categorizers, as shown in Table 1 and 2.The Comparison of the suggested characteristic extraction approach with other approaches in primary data samples is discussed in Table 3. Figure 4 shows that SVM was more efficient in respect of processing duration (processing duration = 38.7 s) with total accuracy when utilizing the identical equipment.

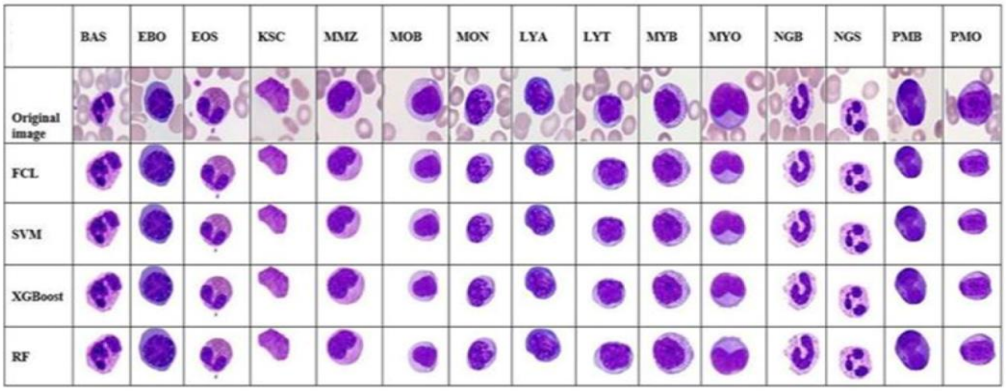

Figure 6. Outcome of WBC Segmentation with the suggested characteristic extraction technique and SVM approach on the primary set of samples.

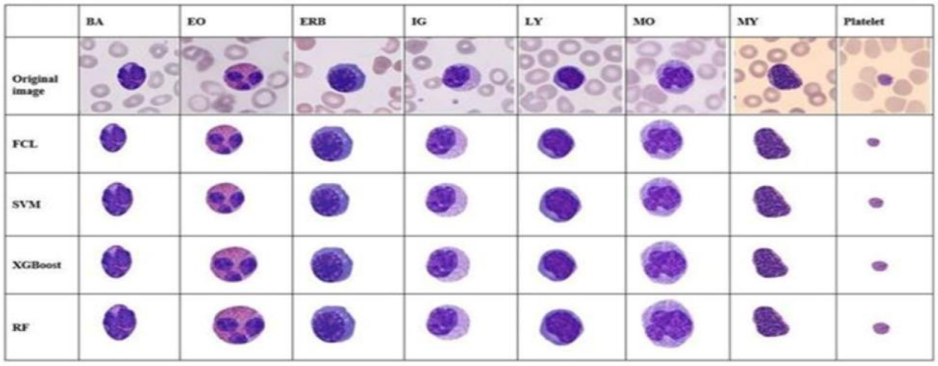

Figure 7. Outcome of various blood plasma delineation with the suggested characteristic retrieval technique via SVM approach on the secondary set of samples.

4.2 Secondary Sample

The secondary sample included 343752 and 175551 blood cells (51.1%) and 168201 non-blood cells (49.9%), respectfully. The suggested characteristic retrieval technique obtained total accuracies of 94.92 percent, 95.47 percent, 96.41 percent, and 95.18 percent, accordingly, utilizing the secondary sample with FCL, RF, SVM, and XGBoost. Table 2 illustrates that the suggested characteristic extraction strategy was stable and gave outcomes that were equivalent between categorizers. The SVM, on the contrary hand, outperformed the previous categorizers and reduced over fitting when opposed to the previous categorizers in figure 5. The outcomes of implementing the suggested characteristic retrieval approach to primary and secondary samples are shown in Figures 6 and 7, accordingly. The suggested approach correctly identified platelet units that were not available in learning with the original sample and recognized all kinds of blood units included in the samples.

Table 3. Comparison of the suggested characteristic extraction approach with other approaches in primary data samples.

	Types of classifiers	**No. Of Features**	**Overall Accuracy**	**Sensitivity**	**Specificity**	**Precision**	**F-score**	**AUC**	**Jaccard index**
M1	FCL	97	0.89	0.94	0.90	0.87	0.90	0.88	0.82
	RF	97	0.91	0.90	0.89	0.94	0.92	0.91	0.85
	SVM	97	0.84	0.86	0.82	0.86	0.86	0.84	0.76
	XGBoost	97	0.89	0.86	0.84	0.94	0.90	0.90	0.82
M2	FCL	98	0.90	0.93	0.91	0.89	0.91	0.89	0.84
	RF	98	0.91	0.91	0.89	0.94	0.92	0.91	0.86
	SVM	98	0.85	0.86	0.83	0.88	0.87	0.85	0.77
	XGBoost	98	0.89	0.86	0.84	0.94	0.90	0.90	0.82
M3	FCL	103	0.91	0.94	0.92	0.90	0.92	0.90	0.85
	RF	103	0.92	0.92	0.90	0.94	0.93	0.92	0.87
	SVM	103	0.90	0.87	0.85	0.94	0.90	0.90	0.93
	XGBoost	103	0.91	0.89	0.87	0.95	0.92	0.92	0.86
M4	FCL	107	0.93	0.93	0.92	0.95	0.94	0.94	0.89
	RF	107	0.95	0.95	0.93	0.96	0.96	0.95	0.92
	SVM	107	0.92	0.90	0.88	0.95	0.92	0.92	0.86
	XGBoost	107	0.93	0.91	0.90	0.95	0.93	0.93	0.88
M5	FCL	108	0.94	0.94	0.93	0.96	0.95	0.95	0.97
	RF	108	0.96	0.96	0.95	0.97	0.96	0.96	0.93
	SVM	108	0.93	0.91	0.89	0.96	0.93	0.93	0.88
	XGBoost	108	0.93	0.91	0.90	0.96	0.94	0.94	0.89
Proposed method	FCL	128	0.97	0.96	0.95	0.99	0.97	0.97	0.95
	RF	128	0.98	0.96	0.95	0.99	0.97	0.97	0.94
	SVM	128	0.97	0.96	0.95	0.99	0.97	0.97	0.95
	XGBoost	128	0.98	0.97	0.96	0.98	0.98	0.97	0.95

5. Conclusion

A generalized WBC characteristic retrieval approach has been developed employing a blended paradigm of traditional image analytics and deep learning techniques with characteristic union. Employing ROIs rather than the full picture, assists in decreasing distortion and eliminating extraneous characteristics, allowing for the creation of a stable and context-free training framework in which the WBC features could be extracted. Considering these as impervious to morphology, hue, as well as coloring fluctuations, 2D convolution stacks produce excellent characteristic retrieval approaches for WBCs. A universal characteristic retrieval paradigm has been established by characteristic merging of solitary as well as piled convolutional planes with varied kernel dimensions and deep grades. The suggested approach identifies 15 different kinds of WBCs, comprising both healthy and cancerous CLL units. The suggested strategy combines the advantages of traditional image

analysis algorithms for ROI retrieval with the advantages of deep learning algorithms for characteristic retrieval. Combination as well as concurrent processing techniques could be used in the later to enhance the suggested system's accuracy while reducing processing duration.

References

[1] K. AL-Dulaimi, J. Banks, K. Nugyen, A. Al-Sabaawi, I. Tomeo-Reyes, and V. Chandran, ''Segmentation of white blood cell, nucleus and cytoplasm in digital haematology microscope images: A Review–challenges, current and future potential techniques,'' IEEE Rev. Biomed. Eng., vol. 14, pp. 290–306, 2021.

[2] L. Bigorra, A. Merino, S. Alférez, and J. Rodellar, ''Feature analysis and automatic identification of leukemic lineage blast cells and reactive lymphoid cells from peripheral blood cell images,'' J. Clin. Lab. Anal., vol. 31, no. 2, Mar. 2017, Art. no. e22024.

[3] Y. Liu and F. Long, ''Acute lymphoblastic leukemia cells image analysis with deep bagging ensemble learning,'' in CNMC Challenge: Classification in Cancer Cell Imaging. Singapore: Springer, 2019, pp. 113–121

[4] J. W. Choi, Y. Ku, B. W. Yoo, J.-A. Kim, D. S. Lee, Y. J. Chai, H.-J. Kong, and H. C. Kim, ''White blood cell differential count of maturation stages in bone marrow smear using dual-stage convolutional neural networks,'' PLoS ONE, vol. 12, no. 12, Dec. 2017, Art. no. e0189259.

[5] N. Baghel, U. Verma, and K. K. Nagwanshi, ''WBCs-Net: Type identification of white blood cells using convolutional neural network,'' Multimedia Tools Appl., vol. 162, pp. 1–17, Sep. 2021.

[6] R. M. Roy and A. P. M., ''Segmentation of leukocyte by semantic segmentation model: A deep learning approach,'' Biomed. Signal Process. Control, vol. 65, Mar. 2021, Art. no. 102385.

[7] K. A. K. Al-Dulaimi, J. Banks, V. Chandran, I. Tomeo-Reyes, and K. N. Thanh, ''Classification of white blood cell types from microscope images: Techniques and challenges,'' Tech. Rep., 2018.

[8] P. Pandey, S. Pallavi, and S. C. Pandey, ''Pragmatic medical image analysis and deep learning: An emerging trend,'' in Advancement of Machine Intelligence in Interactive

Medical Image Analysis. Singapore: Springer, Jan. 2020, pp. 1–18. [Online]. Available: http://www.springer.com/series/16171, doi: 10.1007/978-981-15- 1100-4_1.

[9] S. Asgari Taghanaki, K. Abhishek, J. P. Cohen, J. Cohen-Adad, and G. Hamarneh, ‘‘Deep semantic segmentation of natural and medical images: A review,’’ Artif. Intell. Rev., vol. 4, pp. 1–42, Jun. 2020.

[10] Rakhmadi, ‘‘Connected component labeling using components neighborsscan labeling approach,’’ J. Comput. Sci., vol. 6, no. 10, pp. 1099–1107, Oct. 2010

[11] R. I. Agustin, A. Arif, and U. Sukorini, ‘‘Classification of immature white blood cells in acute lymphoblastic leukemia l1 using neural networks particle swarm optimization,’’ Neural Comput. Appl., vol. 33, no. 17, pp. 10869–10880, Sep. 2021.

[12] S. H. Shirazi, A. I. Umar, N. Haq, S. Naz, M. I. Razzak, and A. Zaib, ‘‘Extreme learning machine based microscopic red blood cells classification,’’ Cluster Comput., vol. 21, no. 1, pp. 691–701, Mar. 2018.

[13] F. Cao, M. Cai, J. Chu, J. Zhao, and Z. Zhou, ‘‘A novel segmentation algorithm for nucleus in white blood cells based on low-rank representation,’’ Neural Comput. Appl., vol. 28, no. S1, pp. 503–511, Dec. 2017

[14] D. López-Puigdollers, V. Javier Traver, and F. Pla, ‘‘Recognizing white blood cells with local image descriptors,’’ Expert Syst. Appl., vol. 115, pp. 695–708, Jan. 2019.

[15] H. A. Elsalamony, ‘‘Detection of anaemia disease in human red blood cells using cell signature, neural networks and SVM,’’ Multimedia Tools Appl., vol. 77, no. 12, pp. 15047–15074, 2018.

[16] M. A. Parab and N. D. Mehendale, ‘‘Red blood cell classification using image processing and CNN,’’ Social Netw. Comput. Sci., vol. 2, no. 2, pp. 1–10, Apr. 2021.

[17] D. T. Nguyen, T. D. Pham, N. R. Baek, and K. R. Park, ‘‘Combining deep and handcrafted image features for presentation attack detection in face recognition systems using visible-light camera sensors,’’ Sensors, vol. 18, no. 3, p. 699, Feb. 2018.

[18] T. Pansombut, S. Wikaisuksakul, K. Khongkraphan, and A. Phon-on, ‘‘Convolutional neural networks for recognition of lymphoblast cell images,’’ Comput. Intell. Neurosci., vol. 2019, pp. 1–12, Jun. 2019

[19] Y. Lu, X. Qin, H. Fan, T. Lai, and Z. Li, ‘‘WBC-Net: A white blood cell segmentation network based on UNet++ and Resnet,’’ Appl. Soft Comput., vol. 101, Mar. 2021, Art. no. 107006.

[20] A. Abdurrazzaq, A. K. Junoh, Z. Yahya, and I. Mohd, ‘‘New white blood cell detection technique by using singular value decomposition concept,’’ Multimedia Tools Appl., vol. 80, no. 3, pp. 4627–4638, Jan. 2021.

[21] N. Khomairoh, R. Sigit, T. Harsono, Y. Hernaningsih, and A. Anwar, ‘‘Segmentation system of acute myeloid leukemia (AML) subtypes on microscopic blood smear image,’’ in Proc. Int. Electron. Symp. (IES), Sep. 2020, pp. 565–570.

[22] R. B. Hegde, K. Prasad, H. Hebbar, and B. M. K. Singh, ‘‘Feature extraction using traditional image processing and convolutional neural network methods to classify white blood cells: A study,’’ Australas. Phys. Eng. Sci. Med., vol. 42, no. 2, pp. 627–638, Jun. 2019

[23] S. Saleem, J. Amin, M. Sharif, M. A. Anjum, M. Iqbal, and S.-H. Wang, ‘‘A deep network designed for segmentation and classification of leukemia using fusion of the transfer learning models,’’ Complex Intell. Syst., Jul. 2021.

[24] V. J. Ramya and S. Lakshmi, ‘‘Acute myelogenous leukemia detection using optimal neural network based on fractional black-widow model,’’ Signal, Image Video Process., vol. 16, no. 1, pp. 229–238, Feb. 2022

[25] A. E. Rad, M. S. M. Rahim, H. Kolivand, and I. B. M. Amin, ‘‘Morphological region-based initial contour algorithm for level set methods in image segmentation,’’ Multimedia Tools Appl., vol. 76, no. 2, pp. 2185–2201, Jan. 2017.

[26] C. D. Ruberto, A. Loddo, and L. Putzu. ‘‘A multiple classifier learning by sampling system for white blood cells segmentation,’’ in Computer Analysis of Images and Patterns. Cham, Switzerland: Springer, 2015.

[27] C. Di Ruberto, A. Loddo, and L. Putzu, ‘‘A leucocytes count system from blood smear images,’’ Mach. Vis. Appl., vol. 27, no. 8, pp. 1151–1160, 2016.

[28] Orlov, Nikita & Chen, Wayne & Eckley, David & Macura, Tomasz & Shamir, Lior & Jaffe, Elaine & Goldberg, Ilya. (2010). Automatic Classification of Lymphoma Images With Transform-Based Global Features. IEEE transactions on information technology in biomedicine : a publication of the IEEE Engineering in Medicine and Biology Society. 14. 1003-13. 10.1109/TITB.2010.2050695.

[29] A. Acevedo, A. Merino, S. Alférez, Á. Molina, L. Boldú, and J. Rodellar, ‘‘A dataset of microscopic peripheral blood cell images for development of automatic recognition systems,’’ Data Brief, vol. 30, Jun. 2020, Art. no. 105474.

[30] V. Andrearczyk and P. F. Whelan, ‘‘Chapter 4—Deep learning in texture analysis and its application to tissue image classification, in Biomedical Texture Analysis, A. Depeursinge, O. S. Al-Kadi, and J.R. Mitchell, Eds. New York, NY, USA: Academic, 2017, pp. 95–129.

[31] A. Zhang, ‘‘Chapter 6: Convolutional neural networks, section 6.4: Multiple input and multiple output channels,’’ in Dive into Deep Learning. 2021.

[32] C. Karabag, J. Verhoeven, N. R. Miller, and C. C. Reyes-Aldasoro, ‘‘Tex- ˇ ture segmentation: An objective comparison between five traditional algorithms and a deep-learning U-Net architecture,’’ Appl. Sci., vol. 9, no. 18, p. 3900, Sep. 2019.

[33] N. Srivastava, G. Hinton, A. Krizhevsky, I. Sutskever, and R. Salakhutdinov, ‘‘Dropout: A simple way to prevent neural networks from overfitting,’’ J. Mach. Learn. Res., vol. 15, no. 56, pp. 1929–1958, 2014.

[34] F. Rosenblatt, ‘‘Principles of neurodynamics. Perceptrons and the theory of brain mechanisms,’’ Cornell Aeronautical Lab Inc, Buffalo, NY, USA, Tech. Rep., 1961.

[35] L. Breiman, ‘‘Random forests,’’ Mach. Learn., vol. 45, no. 1, pp. 5–32, 2001

[36] C. Cortes and V. Vapnik, ‘‘Support-vector networks,’’ Mach. Learn., vol. 20, no. 3, pp. 273–297, 1995.

[37] T. Chen and C. Guestrin, ‘‘XGBoost: A scalable tree boosting system,’’ in Proc. 22nd ACM SIGKDD Int. Conf. Knowl. Discovery Data Mining, Aug. 2016, pp. 785–794.

[38] H. Rezatofighi, N. Tsoi, J. Gwak, A. Sadeghian, I. Reid, and S. Savarese, ‘‘Generalized intersection over union: A metric and a loss for bounding box regression,’’ in Proc. IEEE/CVF Conf. Comput. Vis. Pattern Recognit. (CVPR), Jun. 2019, pp. 658–666.

[39] M. Hossin and M. N. Sulaiman, ‘‘A review on evaluation metrics for data classification evaluations,’’ Int. J. Data Mining Knowl. Manage. Process, vol. 5, no. 2, pp. 1–11, Mar. 2015.

[40] O. O. Koyejo, N. Natarajan, P. K. Ravikumar, and I. S. Dhillon, ‘‘Consistent binary classification with generalized performance metrics,’’ in Proc. NIPS, 2014, pp. 1–9.